ECS Journal of Solid State Science and Technology, **6** (4) P172-P177 (2017)
2162-8769/2017/6(4)/P172/6/$37.00 © The Electrochemical Society

Fluorine Etching in Porous Silicon: An Ab-Initio Molecular Dynamics Study

Marisol R. Arcos and Chumin Wang[z]

Instituto de Investigaciones en Materiales, Universidad Nacional Autónoma de México, C.P. 04510 Mexico City, Mexico

Surface atom removal by fluorine in porous silicon is studied by using the first-principles molecular dynamics based on the density functional theory. The results confirm the preferential <100> crystalline etching direction, in agreement with the experimental results. Moreover, surface silicon atoms are mostly captured by two fluorine and two hydrogen atoms, producing difluorosilane (SiH_2F_2), in contrast to the widely accepted four fluorine-atom capture model. This new capture process could be verified by the infrared spectroscopy.
© 2017 The Electrochemical Society. [DOI: 10.1149/2.0301704jss] All rights reserved.

Manuscript submitted November 8, 2016; revised manuscript received February 3, 2017. Published March 1, 2017.

Silicon is the second most abundant element in the earth crust and the crystalline silicon (c-Si) has been produced with extremely high purity that possesses an indirect energy bandgap of 1.1 eV proper for doped semiconductor devices operating at room temperature.[1] In addition, SiO_2 layers, being one of the best insulators, can be easily grown on the c-Si surface. These are some of the reasons making silicon the base of nowadays electronic industry. Nevertheless, the c-Si has poor optical properties caused by its indirect bandgap, where electronic interband transitions require the assistance of a phonon. In 1990, L. T. Canham reported[2] the first observation of an efficient photo luminescence in porous silicon (PSi) at room temperature, mainly due to the presence of mesoscale pores producing an enlarged bandgap by the quantum confinement and a relaxed momentum selection rule in PSi through structure disorder. An additional feature of PSi is the huge ratio between surface area and volume creating useful applications such as gas and molecular sensors,[3] drug delivery,[4,5] and hydrogen storage.[6,7] Moreover, the refractive index of PSi is a function of porosity making suitable for the design and fabrication of photonic devices[8,9] and solar cell applications.[10]

The production of PSi is simple and cheap; it can be obtained through anodic etching using a c-Si wafer immersed in an ethanoic HF acid solution. The pore shape and size depend on the doping nature and concentration of the wafer, as well as on the applied electrical current intensity.[11] A preferential <100> crystallographic direction for the growth of pores is reported.[12] The most accepted model for the chemical dissolution during the formation of PSi was proposed by Lehmann and Gösele in 1991,[13] in which the etching process can be summarized in Figures 1a–1e, where 1(a) a nucleophilic attack of the Si-H bonds by fluorine ions occurs when silicon is under anodic bias carrying holes to the c-Si surface. This first step of dissolution gives the rise of a Si-F bond in Figure 1b. The second step consists in bonding another fluoride ion at the surface and generating an H_2 molecule, as illustrated in Figure 1c. Due to the large electronegativity of fluorine atom, the Si-Si backbonds are polarized and weakened, making them easy target for the attack of fluoride ions (see Figure 1d). At the final step of dissolution, shown in Figure 1e, a silicon atom is removed from the Si surface releasing a SiF_4 molecule. The resulting Si surface is passivated by hydrogen atoms. Certainly, this model based on the electronegativity concept provides an intuitive description of the silicon dissolution in hydrofluoric acid induced by a hole. However, it does not establish the minimal number of fluoride ions necessary for the dissolution of a silicon atom from c-Si surface. It would also be desirable that this model had a quantum mechanical support to verify, for example, the observed preferential <100> crystallographic pore-growth direction.

On the theoretical side, the ab-initio molecular dynamics (MD) provides a kinetical description of interatomic bond formation, whose interactions calculated by the Density Functional Theory (DFT) offer an accurate starting point to determine atomic motions, in contrast to the use of an effective interaction potential in the classical MD. Furthermore, the ab-initio MD is capable to investigate the reorganization of atoms under experimental conditions, such as at finite temperature and pressure, extending the zero-temperature analysis carried out in standard DFT studies. In fact, silicon was the first system studied by ab-initio MD and its physical properties around the melting point were successfully reproduced.[14] In addition, fluorine etching on the reconstructed Si(100)-2 × 1 surface without hydrogen atoms has been studied by using parametrized[15] and ab initio-derived[16] MD simulations obtaining four fluorine-atom captures. In this article, we report the first ab-initio MD study, up to our knowledge, of the silicon atom removal from the surface of PSi by fluorine atoms.

The rest of this article is organized as follows. In computational method section, we describe the theoretical background of ab-initio MD including thermostats and we specify the used convergence parameters. The fluorine atom bonding on the (100) and (111) surfaces in PSi is studied in fluorine bonding on porous surface section. We report in remotion of silicon by fluorine atoms section the kinetics of silicon-atom dissolution from the surface of PSi. An experimental verification of resulting molecules through vibrational spectroscopies is proposed in the section named a proposal spectroscopic verification. We analyze in penultimate section the electric charge and pore-wall thickness effects on the silicon-atom dissolution and some final remarks are presented in conclusions section.

Computational Method

Ab-initio MD is a powerful method to analyze physical or chemical processes that sensitively depend on the electronic density redistribution along its evolution, for example, chemical bond breaking and formation in adsorption process. The DFT is used to determine the dynamical interaction potential between atoms or molecules, which plays as an input for the MD simulations. In this article we present ab-initio MD calculations within the NVT ensemble, where the temperature is fixed through the Nosé scheme[17] by introducing an additional variable s, representing the thermostat's degree of freedom, to the Hamiltonian. For a given configuration $\{\mathbf{R}_I\}$ of ions, the total energy $E(\{\phi_i\}, \{\mathbf{R}_I\})$ and the single-electron wavefunctions $\{\phi_i\}$ are obtained from the Kohn-Sham equations.[18] The following coupled equations of motion determine the temporal evolution of electronic and ionic degrees of freedom,[19]

$$\mu \frac{d^2\phi_i(\mathbf{r},t)}{dt^2} = -\frac{\delta E}{\delta \phi_i^*(\mathbf{r},t)} + \sum_j \lambda_{ij}\, \phi_j(\mathbf{r},t), \quad [1]$$

$$M_I \frac{d^2\mathbf{R}_I}{dt^2} = -\frac{\partial E}{\partial \mathbf{R}_I} - \frac{M_I}{s}\frac{d\mathbf{R}_I}{dt}\frac{ds}{dt}, \quad [2]$$

and

$$Q\frac{d^2 s}{dt^2} = s\sum_I M_I\left(\frac{d\mathbf{R}_I}{dt}\right)^2 - sgk_BT + \frac{Q}{s}\left(\frac{ds}{dt}\right)^2, \quad [3]$$

[z]E-mail: chumin@unam.mx

Downloaded on 2018-04-30 to IP 132.248.12.226 address. Redistribution subject to ECS terms of use (see ecsdl.org/site/terms_use) unless CC License in place (see abstract).

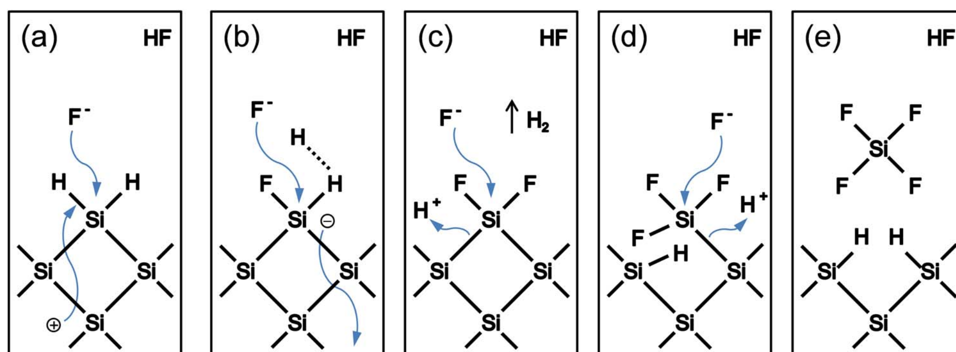

Figure 1. Schematic representation of silicon-atom dissolution from c-Si surface, where (a) a fluoride ion (F^-) assisted by a hole attacks Si-H bond, (b) a Si-F bond is established and a second F^- approaches, (c) another Si-F bond is formed producing a hydrogen molecule (H_2), (d) weakened Si-Si backbonds are attacked by two additional F^-, and finally (e) a SiF_4 molecule is dissolved.

where μ is a fictitious mass or adiabaticity parameter assigned to the orbitals degrees of freedom,[20] Q is a dynamical mass associated to the thermostat, $g = 3N$ being N the number of atoms in the system, and the orthonormality constrains of $\{\phi_i\}$ are introduced by Lagrange multipliers λ_{ij}.

In this work, ab-initio MD calculations were carried out by means of the CASTEP code within Materials Studio using the local density approximation (LDA), CA-PZ functional based on Ceperley-Alder data parameterized by Perdew-Zunger, and Troullier-Martins norm-conserving pseudopotentials.[21] We started from a supercell of 16.3 × 16.3 × 5.4 Å^3 containing 72 crystalline silicon atoms (yellow spheres), where 34 of them were removed to produce a <001> oriented columnar pore and the pore surface was passivated by hydrogen atoms (white spheres), as shown in Figure 2a without the fluorine atoms (blue spheres). The electronic wave functions are expanded in a plane-wave basis set and the MD calculation was performed by using the Nosé-Hoover-Langevin (NHL) thermostat.[22] Most calculation parameters are summarized in Table I.

The calculation parameters of Table I correspond to the ultrafine option of CASTEP. The Nosé-Hoover-Langevin thermostat was chosen since it provided a good temperature control stability for analyzed systems, and the MD time step of 1 fs was selected following the kinetic energy oscillation behavior.

Fluorine Bonding On Porous Surface

In Figure 2a, we placed a fluorine atom inside the pore at such a position equidistant to the (100) and (111) crystalline planes, which is used as the initial configuration for the MD calculations. Figure 2a' is a magnification of 2(a), where $d_2 = 3.0$ Å is the reference distance from the fluorine atom to the silicon atom (Si_2) at the intersection of (100) and (111) planes. Figure 2a" is an x-direction view of 2(a'),

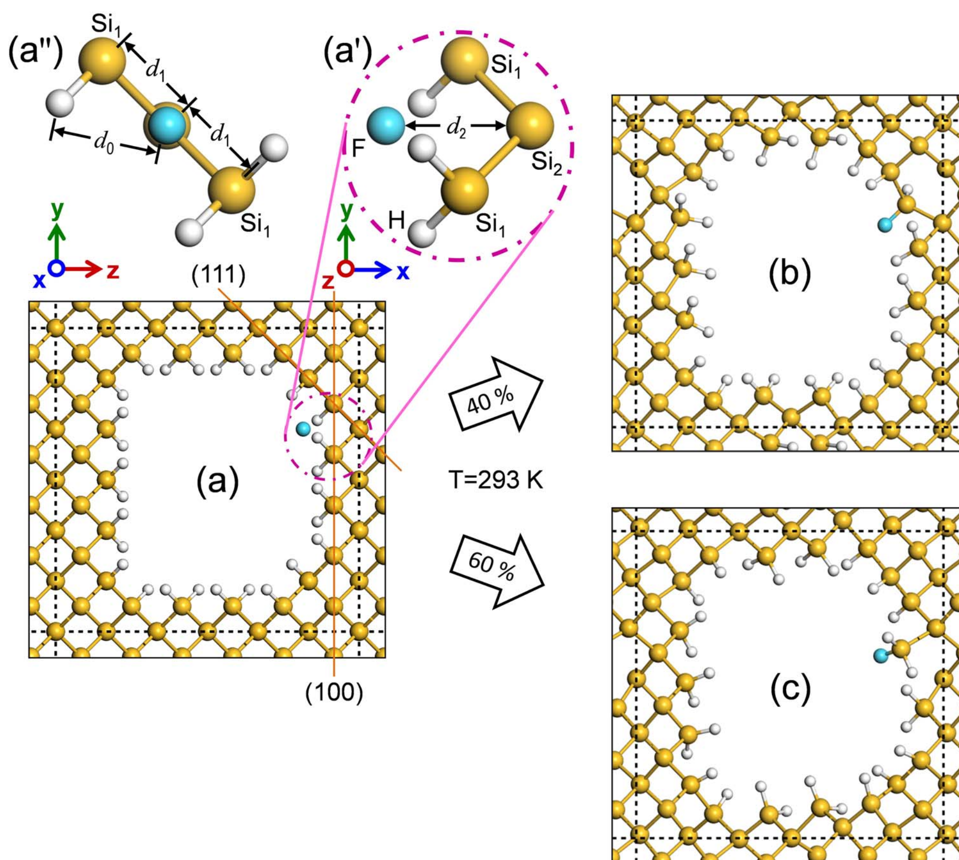

Figure 2. (a) Initial configuration in which a fluorine atom is placed at an equidistant position to both (100) and (111) crystalline planes, (a') a magnification around the fluorine atom, (a") a x-direction view of (a'), (b) and (c) final configurations after 1000 fs with the fluorine atom bonded (111) and (100) surfaces, respectively. At 293 K, the probability to obtain configuration (b) is 60% and 40% for (c).

Downloaded on 2018-04-30 to IP 132.248.12.226 address. Redistribution subject to ECS terms of use (see ecsdl.org/site/terms_use) unless CC License in place (see abstract).

Table I. Summary of the parameters used in the calculations.

	Dynamics	Geometry optimization	Properties
Ensemble	NVT		
Thermostat	NHL		
Temperature	293 K		
Time step	1.0 fs		
Total energy convergence tolerance		5×10^{-6} eV/atom	
Maximum force convergence tolerance		0.01 eV/Å	
Maximum stress convergence tolerance		0.02 GPa	
Maximum displacement convergence tolerance		5×10^{-4} Å	
Self-consistent field tolerance		5×10^{-7} eV/atom	
Energy cutoff (E_c)		940.0 eV	
Electron **k**-point spacing (Δk)		0.07 Å^{-1}	
Phonon **q**-point spacing (Δq)			0.05 Å^{-1}
Force constant convergence tolerance			10^{-5} eV/Å^2
Smearing width			5 cm^{-1}

in which $d_0 = 2.416$ Å and $d_1 = 2.527$ Å respectively denote the distances between fluorine and hydrogen atoms and between fluorine and silicon atoms (Si_1) located on (100) and (111) surfaces.

The MD calculations were performed for ten replications at a temperature of 293 K and the results show that in 60% of the replications the fluorine atom attached on the (100) crystalline surface, while in the rest (40%) replications it bonded to the (111) surface. In addition, we have carried out the same calculations except at a temperature of 4 K and the results reveal that the fluorine atom joined to (100) crystalline surface in all the replications. This qualitatively different result from MD calculations at 293 K and 4 K could be related to the random initial velocity direction of fluorine atom, which is negligible in the case of 4 K. This result is consistent with the observation of preferential <100> pore-grown direction.[12]

Remotion of Silicon By Fluorine Atoms

Let us consider a continuum flux of fluoride ions approaching to the PSi surface as consequence of an applied potential difference during the electrochemical etching. Hence, the dissolution process by fluorine atoms can be divided in two stages. In the first one, we uniformly placed eight fluorine atoms near the PSi surface, as shown in Figure 3a. This initial condition emphasizes the attractive force from a positive charge accumulation on the surface leading fluoride ions toward pore walls. Figure 3b illustrates the bonding of six of eight fluorine atoms at 50 fs. After 90 fs, Figure 3c, all fluorine atoms are attached to the silicon surface and there are four Si-Si backbonds broken due to the high electronegativity of fluorine atoms. Furthermore, we observed seven broken Si-Si backbonds at 1000 fs, as displayed in Figure 3d. In the second stage, Figure 3e, four more fluorine atoms are added at a distance of 2.2 Å from those silicon atoms bonded to a fluorine atom. Figures 3f and 3g illustrate the bonding of four additional fluorine atoms and the capture of two silicon atom, respectively. Finally, we observe the formation of two molecules of SiH_2F_2 in Figure 3h. It is important mentioning that the number of fluorine atoms was chosen in accordance to an electrolyte containing 25% of pure HF acid. In addition, with the same initial conditions we have performed five replications obtaining essentially the same

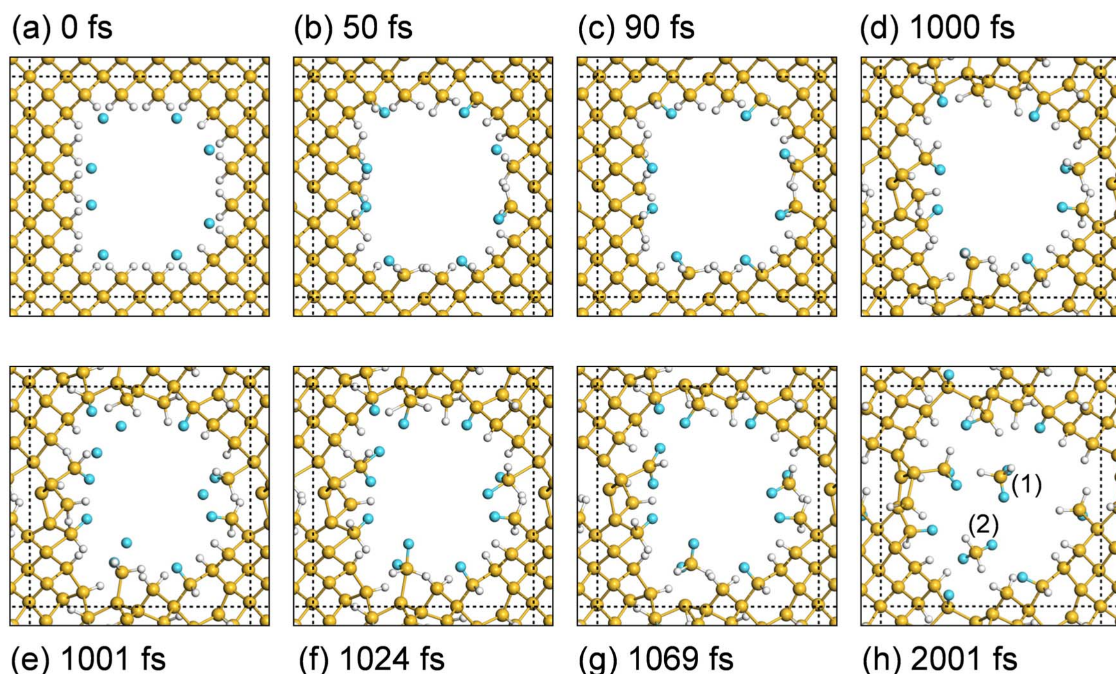

Figure 3. (a) A uniform distribution of eight F atoms are placed inside PSi near to the surface, (b) they approach to the surface and some F-Si bonds are established, (c) all these atoms are attached to the Si surface and (d) after 1000 fs seven Si-Si backbonds are broken. In addition, (e) four more F atoms are added, (f) they bond to the surface Si atoms, (g) two Si atoms are captured and finally, (h) two molecules of SiH_2F_2 are produced and labeled by (1) and (2).

Downloaded on 2018-04-30 to IP 132.248.12.226 address. Redistribution subject to ECS terms of use (see ecsdl.org/site/terms_use) unless CC License in place (see abstract).

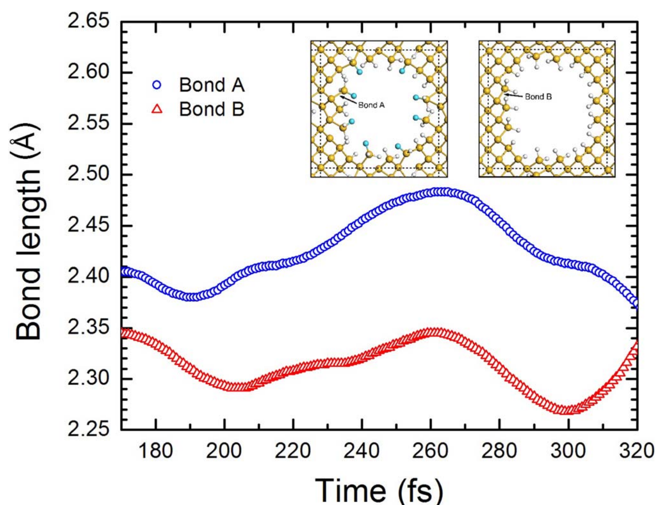

Figure 4. Si-Si backbond lengths versus simulation time with (blue circles) and without (red triangles) the presence of fluorine atoms. Insets illustrate the PSi supercells, where lengths of bond A and bond B were calculated with and without fluoride-ion, respectively.

results, whose differences are originated by the stochastic nature of NHL thermostat.

In order to analyze the effects of fluorine-atom electronegativity, we have monitored a Si-Si backbond length by comparing bonds A and B in the insets of Figure 4, which respectively correspond the PSi with and without the presence of fluorine atom. The lengths of bond A (blue circles) and bond B (red triangles) as functions of simulation time, between 170 and 320 fs of the MD shown in Figure 3, are illustrated in Figure 4. Notice that bond A is significantly larger than bond B, which suggest the weakening of Si-Si backbond due to the presence of fluorine atom. In general, there is an inversely proportional relationship between the bond length and the dissociation energy, as observed in carbon-carbon bonds.[23]

A Proposal of Spectroscopic Verification

The results presented in Figure 3 confirm the essential of the widely accepted PSi formation model proposed by Lehmann and Gösele, except for the resulting molecules, i.e., ab-initio MD suggests the formation of difluorosilane (SiH_2F_2) instead of SiF_4. In order to investigate the possibility of detecting the presence of this molecule, we further calculate vibrational density of states, Raman and infrared spectra of PSi with and without such molecule. The vibrational calculations were performed within the Density Functional Perturbative Theory (DFPT), which is based on the DFT ground-state electron charge density and the linear response approximation to a distortion of nuclear geometry.[24] The DFPT has been successfully applied to the adsorption study of oxygen atoms in PSi verified by infrared spectroscopy.[25] Starting from the MD final configuration, Figure 3h, we have carried out a geometry optimization using parameters of Table I before the DFPT calculations. Figures 5 show phonon density of states (DOS) for PSi (a) with and (b) without SiH_2F_2, as well as (c) phonon DOS of a single SiH_2F_2 inside a supercell of $20 \times 20 \times 20$ Å^3. It is important to note the peaks at frequencies 939.1, 959.4, 2195.9 and 2213.8 cm^{-1} in Figure 5c, as well as their presence in Figure 5a and absence in Figure 5b. The phonon modes corresponding to these peaks could be detected by vibrational spectroscopy, such as Raman scattering and infrared absorption.

Figure 6 shows the Raman spectra of (a) PSi with SiH_2F_2, (b) PSi without SiH_2F_2 and (c) a single SiH_2F_2, calculated using an incident wave length of 514.5 nm and a Lorentzian peak profile. Notice that the Raman response intensity of solids is two orders of magnitude larger than that of molecules. This fact is also observed in other

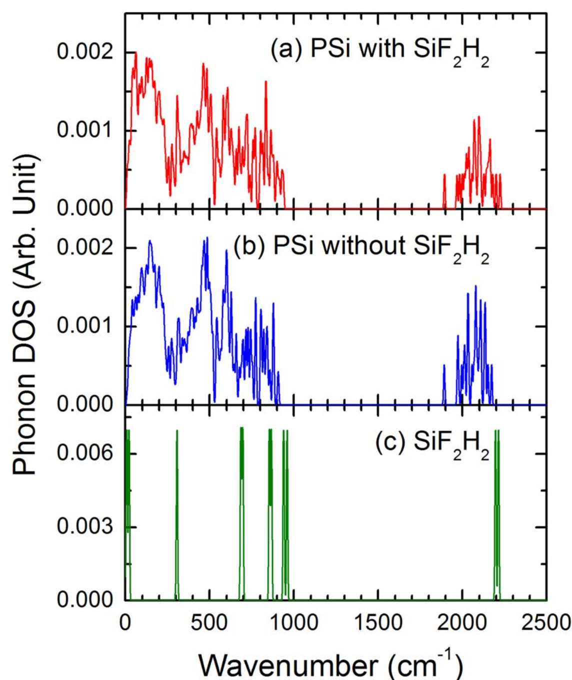

Figure 5. Phonon density of states (DOS) of (a) PSi with SiH_2F_2, (b) PSi without SiH_2F_2 and (c) a single SiH_2F_2.

compounds.[26] In consequence, the Raman spectra with and without SiH_2F_2 are essentially the same, since the molecule contribution is much smaller than the solid one.

Given that Raman response is not sensitive to the presence of SiH_2F_2, we further calculate the infrared spectra for the same systems of Figure 6. The results of infrared absorption are shown in Figure 7. Note the spectral shape similarity between the vibrational density of

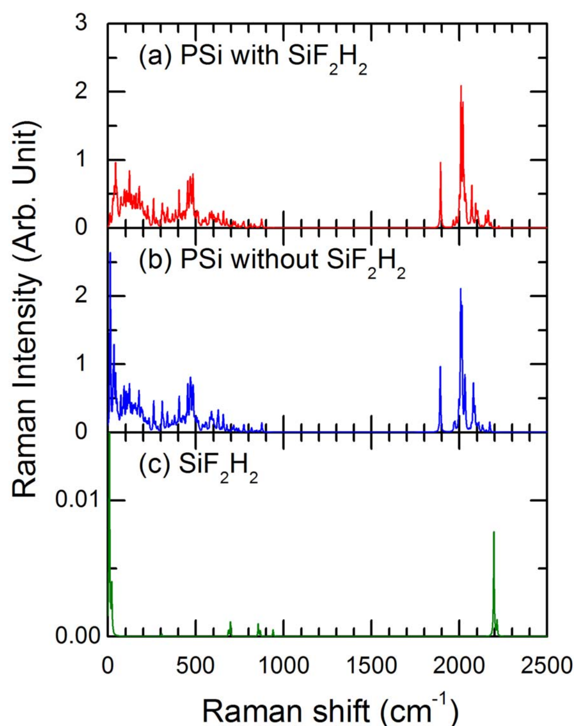

Figure 6. Raman response spectra of (a) PSi with SiH_2F_2, (b) PSi without SiH_2F_2 and (c) a single SiH_2F_2.

Downloaded on 2018-04-30 to IP 132.248.12.226 address. Redistribution subject to ECS terms of use (see ecsdl.org/site/terms_use) unless CC License in place (see abstract).

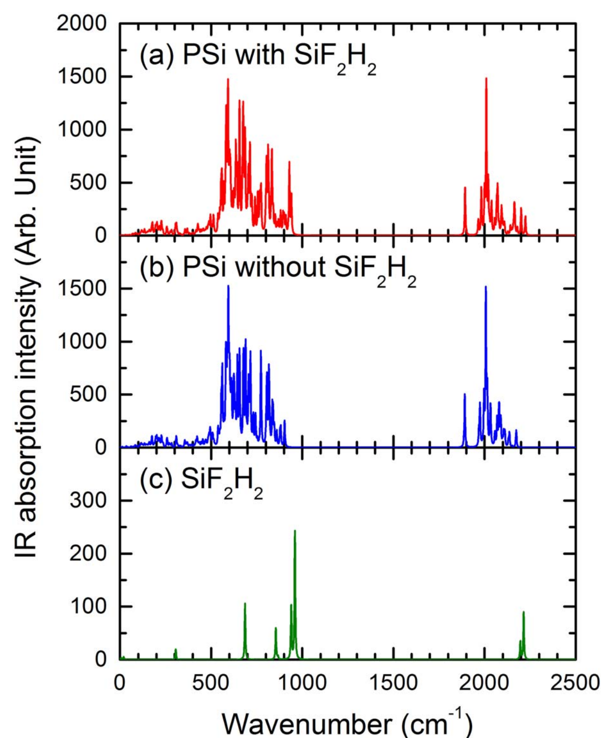

Figure 7. Infrared absorption intensity (a) PSi with SiH_2F_2, (b) PSi without SiH_2F_2, and (c) SiH_2F_2.

states and infrared spectra, except for the region with wavenumbers under 500 cm^{-1}, in contrast to the stronger Raman response in this zone. This fact is consistent with the mutual exclusion rule.[27] Observe the vibrational modes around 920 and 2200 cm^{-1} in Figure 7a, which come from the molecule SiH_2F_2, as illustrated in Figure 7c.

In Table II, a complete list of nine vibrational modes of molecules (1) and (2) shown in Figure 3h is compared with experimental data measured in a gas of SiH_2F_2.[28] These molecular vibrational modes in PSi have been determined by analyzing the displacement vectors of each atom in the system. Notice that the relative error between theoretical and experimental results in Table II is less than 10%, which contains a systematic shift to low wavenumber of theoretical results in comparison with the experimental ones, mainly due to the dielectric constant of PSi in the IR absorption calculations. Hence, the vibrational modes obtained from ab-initio DFPT calculations have a good consistency with experimental results, which only confirm the accuracy of IR-spectrum numerical calculations.

Charge and Pore-Wall Thickness Effects

In this section we study the electric charge and pore-wall thickness effects on the dissolution process in PSi by using a larger supercell of 21.7 × 21.7 × 5.4 Å^3 with 128 silicon atoms, and we remove 34 of them producing the same columnar pore as in Figure 3a. Figures 8b, 8b' and 8b" illustrate the initial configurations with one positive, neutral and negative in units of the electron charge, whose densities of states (DOS) were shown in Figures 8a, 8a' and 8a", respectively. The number of valence electrons was calculated by integrating the DOS for each case, leading to 403, 404 and 405 electrons, as indicated above Figures 8a, 8a' and 8a". Eight fluorine atoms are placed with the same distribution around pore surface as in Figure 3a. The ab-initio MD calculations were performed by using the parameters described in Table I and the same two-stages capture procedure illustrated in Figure 3, except a shorter simulation time due to computational limitations. Actually, this reduction of simulation time has minor effects on the results, since silicon atoms at the pore surface were removed by fluorine and hydrogen ones at early stages of simulation, as seen in Figures 8e, 8e' and 8e". Observe that all the fluorine atoms are bonded to PSi surface at 45 fs in Figure 8c, in contrast to two free fluorine atoms appeared in Figures 8c' and 8c" at the same simulation time, originated by the difference in total electric charge of the structures. Notice also that the increase of pore-wall thickness gives the rise of a better structure stability in comparison with Figure 3. Moreover, the silicon atom capture by two-fluorine and two-hydrogen atoms is observed in all analyzed cases, except the number of removed silicon atoms from PSi surface, i.e., three captures for the positive-charge case, two for the neutral case, and only one for the negative-charge case. It is worth mentioning that for each case we have performed at least three replications, whose results are slightly different due to the NHL thermostat used.

Conclusions

In this work, an ab-initio MD calculation has been carried out to study the etching process in porous silicon (PSi). We started from a supercell with a columnar pore fully passivated by hydrogen atoms and a fluorine atom was placed on an equidistant site to the (100) and (111) crystalline planes. The ab-initio MD results confirm that the pore grows along <100> crystalline direction with a preference of 100% at 4 K and 60% at 293 K. In order to study the removal of silicon atoms from PSi surface, eight fluorine atoms were uniformly placed close to the silicon surface, in consideration of the usual HF acid concentration in the electrolyte and the potential difference applied during etching process. Four fluorine atoms were additionally introduced after 1000 fs, simulating a continuum flux of HF acid. ab-initio MD results suggest the formation of difluorosilane (SiH_2F_2) as the dominant process of Si atom removal from the PSi surface, in contrast to the widely accepted PSi formation model proposed by Lehmann and Gösele. It is worth mentioning that this calculation has been performed five times and each of them reaches to a different final configuration due to the use of NHL stochastic thermostat. However, the molecule SiH_2F_2 is always the main resulting molecule in all analyzed cases with different charges and pore-wall thickness.

We further analyze the possibility of an experimental verification by vibrational spectroscopy to ensure the presence of SiH_2F_2 as the main product during the etching process. The vibrational analysis

Table II. Vibrational frequencies of SiH_2F_2 in PSi (cm^{-1}).

Vibrational modes	SiH_2F_2 (1) (cm^{-1})	SiH_2F_2 (2) (cm^{-1})	Experimental data[28]
SiF_2 scissoring	306.64	303.97	322.85
SiH_2 rocking	671.03	678.20	730.0
SiH_2 twisting	721.95	715.38	730.0
SiF_2 symmetric stretching	834.5	833.36	869.6
SiH_2 wagging	860.72	861.98	903.4
SiH_2 scissoring	909.89	894.36	981.7
SiF_2 anti-symmetric stretching	940.30	929.00	981.0
SiH_2 symmetric stretching	2179.95	2162.94	2245.7
SiH_2 anti-symmetric stretching	2200.95	2224.31	2250.5

Downloaded on 2018-04-30 to IP 132.248.12.226 address. Redistribution subject to ECS terms of use (see ecsdl.org/site/terms_use) unless CC License in place (see abstract).

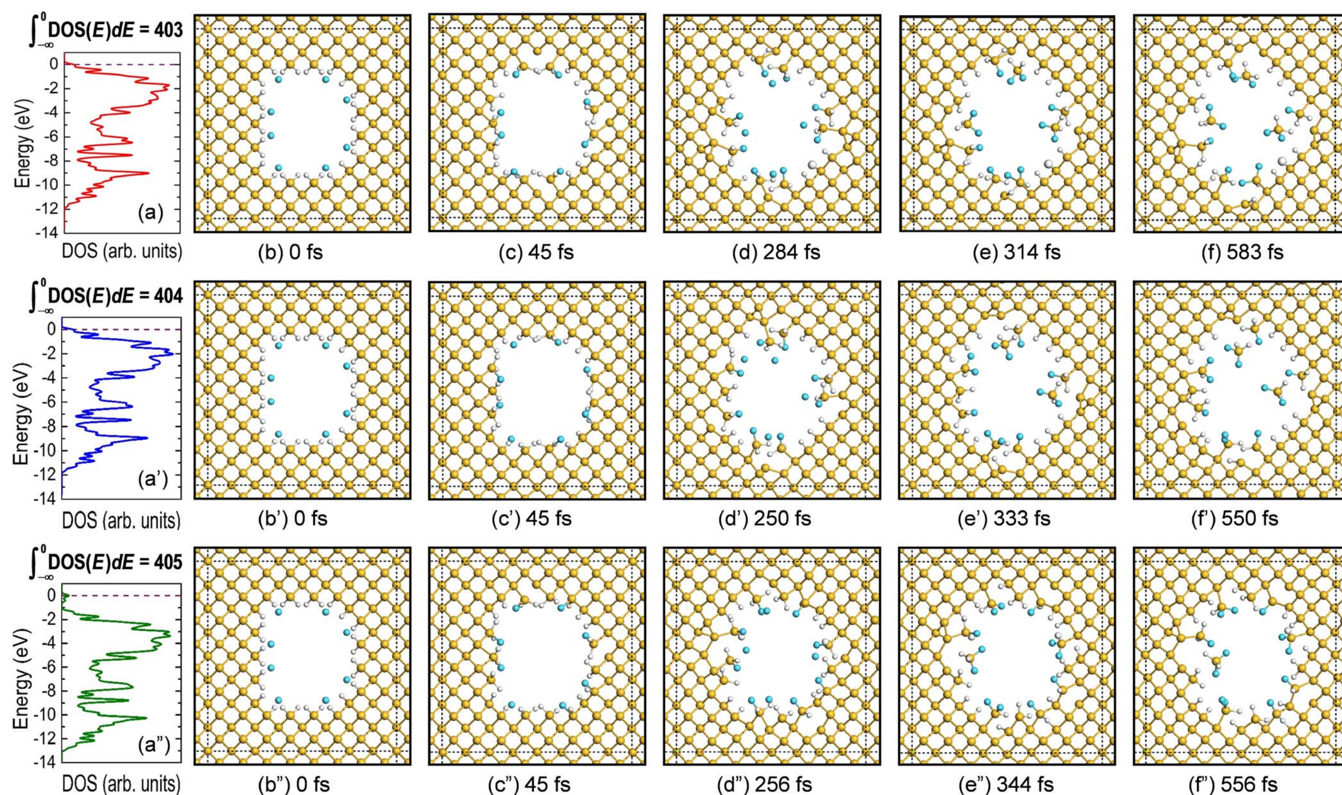

Figure 8. Ab-initio MD performed on a supercell of 21.7 × 21.7 × 5.4 Å^3 with the same pore and following the same two-stage capture procedure as in Figure 3, except that now the structure has (b-f) one absent, (b'-f') zero absent and (b"-f") one extra electron with respect to the positive charges in the supercell, as respectively illustrated by the integrated values of the density of states (DOS) shown in (a), (a') and (a") obtained for the initial structure without fluorine atoms.

carried out within the DFPT scheme suggests an in-situ measurement using infrared absorption spectroscopy, as done in the experimental study of SiH_2F_2 on Si surface,[29] since the molecule could be chemically unstable in the HF electrolyte. Finally, this study provides a quantum mechanical background for the etching process model in PSi and the ab-initio MD approach used seems to be appropriate for studying the silicon removal process, because the system size and simulation time limitations inherent of ab-initio MD methods are not relevant in this study. The present work could be extended to include hydrogen ions, water and ethanol molecules in a larger silicon pore, which is currently under study.

Acknowledgments

This work has been partially supported by CONACyT-252943 and UNAM-DGAPA-PAPIIT Project IN116317. Computations were performed at Miztli of DGTIC-UNAM, where the technical assistance of Yolanda Flores is fully appreciated.

References

1. V. Lehmann, *Electrochemistry of silicon: instrumentation, science, materials and applications*, p. 5, Wiley-VCH Verlag, Weinheim, (2002).
2. L. T. Canham, *Appl. Phys. Lett.*, **57**, 1046 (1990).
3. H. Kim and K. Lee, *Sens. Actuators B: Chemical*, **219**, 10 (2015).
4. S. J. P. McInnes, E. J. Szili, S. A. Al-Bataineh, R. B. Vasani, J. Xu, M. E. Alf, K. K. Gleason, R. D. Short, and N. H. Voelcker, *Langmuir*, **32**, 301 (2016).
5. N. H. Maniya, S. R. Patel, and Z. V. P. Murthy, *Superlattices Microstruct.*, **85**, 34 (2015).
6. X. Song and J. Wu, *Adv. Mater. Res.*, **415**, 2322 (2012).
7. S. Chandrasekaran, T. Nann, and N. H. Voelcker, *Nano Energy*, **17**, 308 (2015).
8. D. R. Huanca and W. J. Salcedo, *Phys. Status Solidi A*, **212**, 1975 (2015).
9. C. Pacholski, *Sensors*, **13**, 4694 (2013).
10. M. Aliaghayee, H. G. Fard, and A. Zandi, *J. Porous Mater.*, **22**, 1617 (2015).
11. R. Cisneros, H. Pfeiffer, and C. Wang, *Nanoscale Res. Lett.*, **5**, 686 (2010).
12. M. Christophersen, J. Carstensen, S. Rönnebeck, C. Jäger, W. Jäger, and H. Föll, *J. Electrochem. Soc.*, **148**, E267 (2001).
13. V. Lehmann and U. Gösele, *Appl. Phys. Lett.*, **58**, 856 (1991).
14. M. Parrinello, *Solid State Commun.*, **102**, 107 (1997).
15. A. Darcy, A. Galijatovic, R. Barth, T. Kenny, K. D. Krantzman, and T. A. Schoolcraft, *J. Mol. Graphics*, **14**, 260 (1996).
16. C. J. Wu and E. A. Carter, *J. Am. Chem. Soc.*, **113**, 9061 (1991).
17. S. Nosé, *J. Chem. Phys.*, **81**, 511 (1984).
18. W. Kohn and L. J. Sham, *Phys. Rev.*, **140**, A1133 (1965).
19. I. Stich, R. Car, and M. Parrinello, *Phys. Rev. Lett.*, **63**, 2240 (1989).
20. D. Marx and J. Hutter, *Ab-initio Molecular Dynamics: Basic Theory and Advanced Methods*, p. 30, Cambridge University Press (2009).
21. S. J Clark, M. D. Segall, C. J. Pickard, P. J. Hasnip, M. I. J. Probert, K. Refson, and M. C. Payne, *Z. Kristallogr.*, **220**, 567 (2005).
22. B. Leimkuhler, E. Noorizadeh, and F. Theil, *J. Stat. Phys.*, **135**, 261 (2009).
23. A. A. Zavitsas, *J. Phys. Chem. A*, **107**, 897 (2003).
24. S. Baroni, S. de Gironcoli, and A. Dal Corso, *Rev. Mod. Phys.*, **73**, 515 (2001).
25. P. Alfaro, A. Palavicini, and C. Wang, *Thin Solid Films*, **571**, 206 (2014).
26. J. R. Lombardi and R. L. Birke, *J. Phys. Chem. C*, **118**, 11120 (2014).
27. J. M. Hollas, *Modern Spectroscopy*, p. 173, 4th ed., John Wiley & Sons (2004).
28. J.-F. D'Eu, J. Demaison, and H. Bürger, *J. Mol. Spectrosc.*, **218**, 12 (2003).
29. M. Niwano, T. Miura, Y. Kimura, R. Tajima, and N. Miyamoto, *J. Appl. Phys.*, **79**, 3708 (1996).

Downloaded on 2018-04-30 to IP 132.248.12.226 address. Redistribution subject to ECS terms of use (see ecsdl.org/site/terms_use) unless CC License in place (see abstract).